Scaling properties of turbulence driven shear flow

Z. Yan,[1,2] G. R. Tynan,[1] C. Holland,[1] M. Xu,[1] S. H. Muller,[1] and J. H. Yu[1]
[1]*University of California, San Diego, La Jolla, California 92093, USA*
[2]*University of Wisconsin-Madison, Madison, Wisconsin 53706, USA*

(Received 23 July 2009; accepted 17 November 2009; published online 13 January 2010)

The characteristics and scaling properties of the turbulence driven shear flow are investigated in a cylindrical laboratory plasma device. For a given plasma pressure, the density fluctuation amplitude and radial particle flux increase with the applied magnetic field. Strong flow shear is found to coexist at high magnetic fields (>700 G) with ~ 10 kHz drift wave turbulence, but not at low magnetic fields (<700 G). The absolute value of the divergence of the turbulent Reynolds stress at the shear layer is shown to increase with the magnetic field as well. For a fixed magnetic field, the shear flow is found to decrease as the discharge gas pressure is increased. The density fluctuation amplitude and divergence of the turbulent Reynolds stress also decrease with the plasma pressure. For both situations the cross phase between the radial and azimuthal components of the velocity is found to be a key factor to determine variations in the turbulent Reynolds stress at different magnetic fields and discharge pressures. The results show that the generation of the shear flow is related to the development of specific frequency components of the drift wave turbulence for a variety of plasma conditions. The linear stability analysis shows that the observed variation in the turbulence and shear flow with magnetic field is also consistent with a critical gradient behavior. © *2010 American Institute of Physics*. [doi:10.1063/1.3276521]

I. INTRODUCTION

The mechanism of shear flow generation is of great interest since it is thought to regulate turbulent transport and is also a potential candidate for the transition to high confinement regime in tokamaks.[1,2] One example of experimental evidence for coupling between sheared flow development and an increase in the level of edge turbulence has been provided in TJ-II stellarator.[3] Previous work on the linear cylindrical plasma device Controlled Shear Decorrelation Experiment (CSDX) has shown that the observed shear flow is consistent with the turbulent Reynolds stress[4] and the cross phase between the turbulent radial and azimuthal velocity fluctuations played a key role in determining the shape of the Reynolds stress profile.[5] These previous results were all obtained at a magnetic field of 1000 G, well above the magnetic field threshold for the onset of drift wave turbulence in the device.[6] In previous work, it has also been shown that the magnetic field strength is an important control parameter governing the development of drift wave turbulence in the CSDX device.[6] As the magnetic field is increased from 400 to 1000 G, the plasma drift wave fluctuations evolve from narrow-band (i.e., frequency width much smaller than the wave frequency) coherent wavelike perturbations that were consistent with collisional drift turbulence linear eigenmodes into a state of weak drift turbulence that was characterized by broadened frequency and wave number spectra that still roughly follow the linear dispersion relation (and hence these fluctuations were characterized as being in a state of weak turbulence). The role of the magnetic field acting as a control parameter for the transition to drift turbulence has also been reported in many other papers (see, e.g., Refs. 7 and 8). This effect is attributed to the reduction in the ion-ion collisional viscosity $\mu_{ii} \propto \rho^2 \nu_{ii} \propto 1/B^2$ that occurs at higher magnetic fields. As the viscosity is reduced, the convective derivative, and hence the nonlinear interactions that are mediated by it, becomes more prominent in the fluid conservation equations[6] in a manner analogous to the transition to turbulence that occurs in neutral fluid turbulence when the Reynolds number is increased. Given these earlier results, and the observations that the turbulence and zonal flows form a nonlinearly coupled system, the question naturally arises: How does this coupled system evolve as the magnetic field is increased in this laboratory experiment? The neutral gas pressure has also been used to control the transition to turbulence.[9,10]

Ion-neutral drag due to collisions between these species can also act to damp out turbulent-driven shear flows[4] in a process that is analogous to the damping of zonal flows in toroidal devices due to collisions between trapped and passing ions,[11] and is thus of fundamental interest as well. Therefore, it is interesting to study how the shear flow and its generation change when the flow damping is also changed. There is no straightforward way to study the scaling properties of the shear flow generation with magnetic field or flow damping in larger confinement devices, and the results discussed here provide a needed experimental study of the onset of turbulent-driven shear flows in plasmas, as well as the first controlled study of the effect of flow damping on these flows.

The rest of the paper is organized as follows. In Sec. II we discuss the magnetic field scaling properties of the turbulence driven shear flow. In Sec. III we discuss the pressure scaling properties of the turbulence driven shear flow. In Sec. IV we discuss linear stability analysis, and lastly, in Sec. V we review and summarize our results.

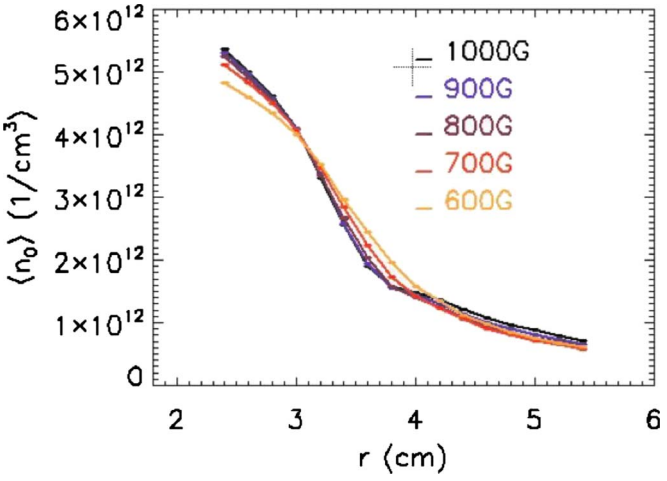

FIG. 1. (Color online) Equilibrium plasma density profile for different magnetic fields.

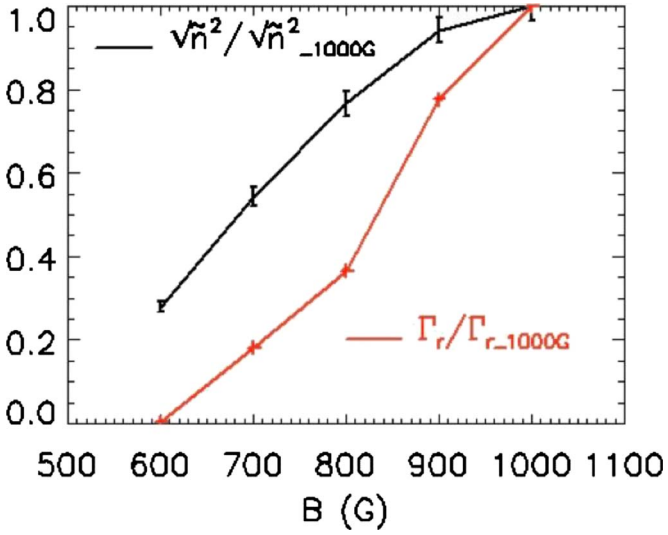

FIG. 2. (Color online) Density fluctuation amplitude (solid line) and radial particle flux (solid line and symbol +) at 3.18 mTorr for different magnetic fields. Each is normalized by the corresponding value at 1000 G magnetic field.

II. MAGNETIC FIELD SCALING OF THE TURBULENCE DRIVEN SHEAR FLOW

The experiments presented here are carried out in the CSDX linear cylindrical plasma device. It has an overall length of 2.8 m and around 20 cm in diameter. The vacuum chamber is surrounded by a set of magnetic coils that can generate uniform magnetic fields along the axial direction (denoted here as the z direction) varying from 400 up to 1000 G. The plasma is generated by a rf source power at 13.56 MHz. The typical operation condition is at 3 mTorr gas pressure, 1000 G magnetic field, and 1.5 kW source power for the argon plasma. A detailed description of the machine can be found elsewhere.[6,12] A dual 3×3 array of Langmuir probes is used to measure the plasma density and floating potential at several radial locations for various magnetic fields and plasma pressure conditions. A detailed description of this probe can be found in Refs. 5 and 13. The radial and azimuthal separations of the probe tips can provide measurements of Reynolds stress $-\langle\tilde{v}_r\tilde{v}_\theta\rangle=\langle\tilde{E}_r\tilde{E}_\theta/B^2\rangle$, where the electric field components are measured from the appropriate gradient in the floating potential. A time delay estimation technique[14] is applied to dual azimuthally displaced density fluctuation measurements to obtain a radial profile of the azimuthal velocity fields.

Figure 1 provides a plot of the time-averaged radial plasma density profiles for different magnetic fields obtained from the ion saturation current measurements, while Fig. 2 provides the density fluctuation amplitude and radial particle flux near the maximal density gradient location ($r=3$ cm). All the data are taken at an argon fill pressure of 3.18 mTorr and a source power input of 1.5 kW. The density fluctuations and radial particle flux are all normalized by the corresponding values at 1000 G magnetic field. The results show that plasma time-averaged density gradient increases slightly as the magnetic field is increased, but that this gradient increase appears to saturate once the magnetic field exceeds 800 G. The density fluctuation amplitude and the radial particle flux both become significant once the magnetic field exceeds 600 G, and they rapidly increase as the magnetic field is increased toward 1000 G, consistent with previous results.[6]

Figure 3(a) shows the radial profile of the time-averaged azimuthal velocity in a 3.18 mTorr, 1.5 kW argon discharge at five different magnetic fields computed as we have discussed elsewhere.[15] Figure 3(b) shows the shearing rate computed from these data at $r=3.8$ cm for different magnetic fields. The result shows that the shear flow exists when the magnetic field is $B\geqslant700$ G, while for lower magnetic fields (600 G is shown in the figure), the fluctuations propagate with nearly a constant azimuthal velocity. The power spectra of both ion saturation current and floating potential fluctuations obtained at the shear layer ($r=3.8$ cm) are shown in Fig. 4, with the dashed line indicating the density fluctuation spectrum and the solid line indicating the floating potential fluctuation spectrum. Several features are of note. First, as the magnetic field is raised, the low frequency (<2 kHz) potential fluctuation power increases substantially. We interpret this as representing the onset of the azimuthally symmetric shear flow; the finite width of this frequency component corresponds to slow variations in this shear flow that has been documented in other work.[15] Second, as the magnetic field begins to exceed 700 G, a new set of fluctuations in the frequency range of $\sim7-8$ kHz appears. As the magnetic field increases further, these fluctuations increase in frequency. When the magnetic field reaches 1000 G, these fluctuations have frequencies of $\sim8-10$ kHz. As was shown in an earlier bicoherence analysis,[15] at 1000 G it is this frequency range that is most strongly phase coherent (and thereby capable of exchanging energy) with the slowly varying shear flow. Compared with the results shown in Fig. 3, and the results from previous work[15] that showed a slow temporal variation in the shear flow and also a strong phase coherent coupling between this low frequency flow and the drift wave fluctuations at ~10 kHz, these observations suggest that the onset of the shear flow is related to the devel-

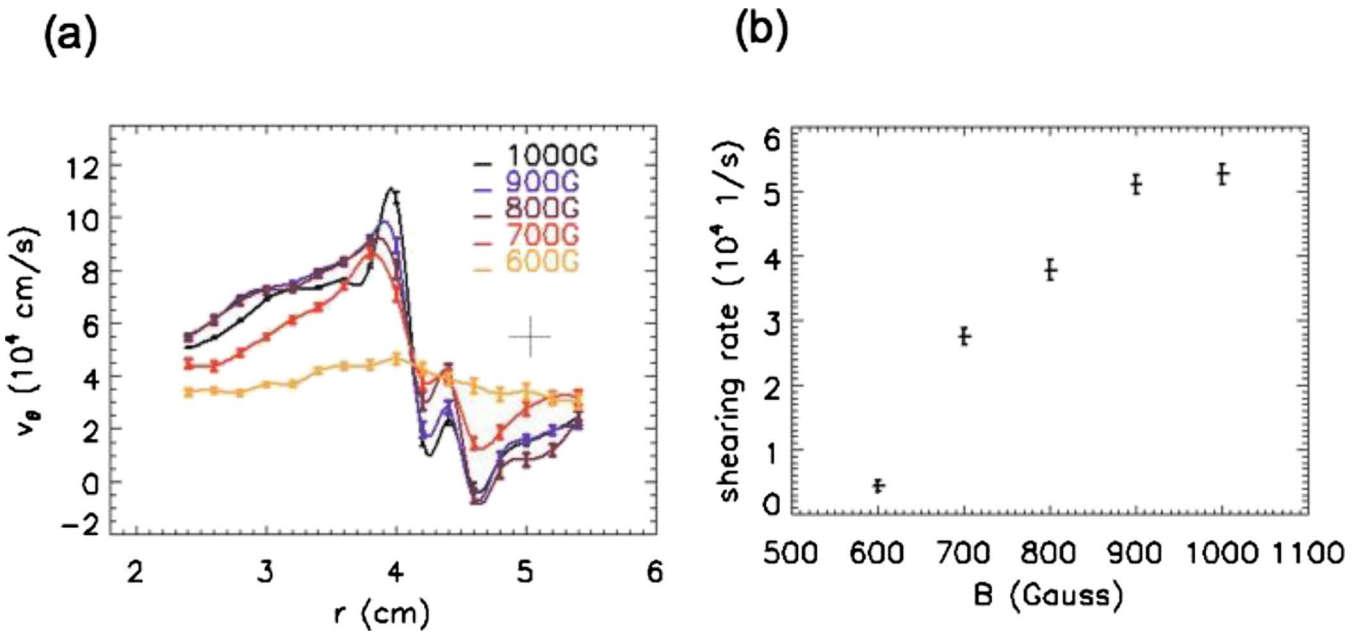

FIG. 3. (Color online) (a) Time-averaged azimuthal velocity fields for different magnetic fields. (b) Shearing rate at shear layer for different magnetic fields.

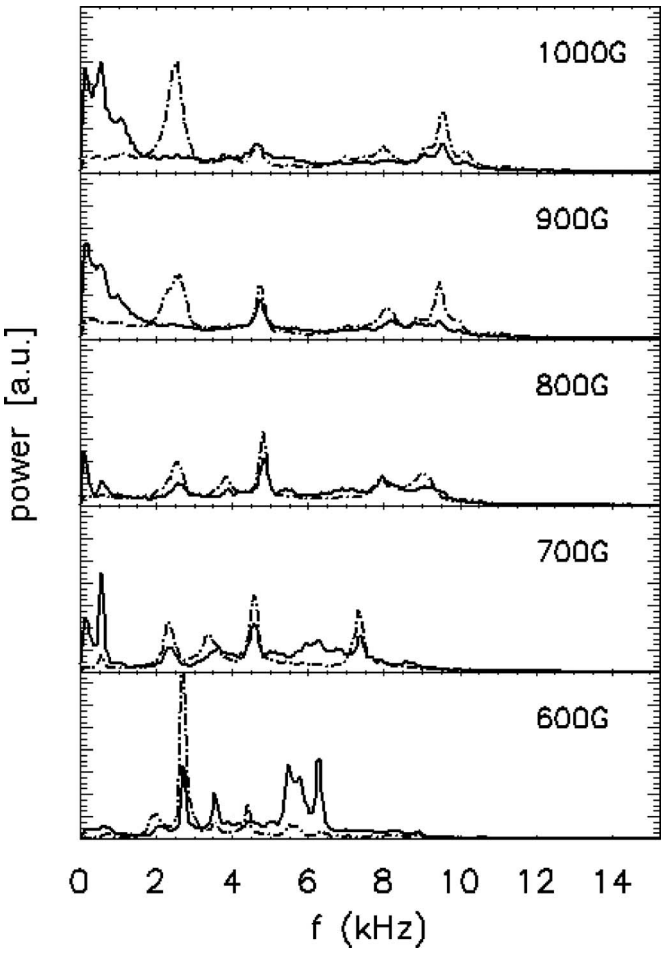

FIG. 4. Power spectra of density fluctuations (dashed line) and floating potential (solid line) at the shear layer (~3.8 cm) with $P=3.18$ mTorr for different magnetic fields.

opment of the ~7–8 kHz fluctuations at $B\sim700$ G and then the subsequent evolution of those fluctuations to ~9–10 kHz as the magnetic field is raised to $B=1000$ G. The amplitude of the low frequency floating potential oscillation, which is associated with the slowly varying shear flow, is also proportional to the magnetic field. Taken together, these results indicate that as the magnetic field is increased, the drift wave turbulence amplitude increases, the nonlinear coupling between the shear flow and the weak drift turbulence increases, and the strength of the shear flow increases. This scaling is qualitatively consistent with the theoretical picture of turbulence driven shear flow that is summarized in a review paper by Diamond *et al.*[1]

If the shear flow is driven by the fluctuations, as shown previously[4,15] and supported by the above results, then the divergence of the turbulent Reynolds stress should also be small or zero for $B<700$ G, and then should increase once the magnetic field exceeds this threshold. In particular, from theory and previous experimental studies for the statistical properties of the turbulent Reynolds stress,[5] we know that the negative divergence of turbulence Reynolds stress $\nabla\cdot(\tilde{v}_r\tilde{v}_\theta)$ will reinforce the shear flow. Therefore, it is interesting to look at the evolution of $\nabla\cdot(\tilde{v}_r\tilde{v}_\theta)$ with magnetic fields. In Fig. 5, the symbols denote the absolute values of the $\nabla\cdot(\tilde{v}_r\tilde{v}_\theta)$ at the shear layer (~3.8 cm) for different magnetic fields. The results show that the amplitude of $\nabla\cdot(\tilde{v}_r\tilde{v}_\theta)$ is small at 600 G and then increases with magnetic field, consistent with expectations. We also note that at low magnetic field of 600 G, there is a finite divergence of the turbulent Reynolds stress, but there is no shear flow at that condition. This discrepancy is because the ion gyrofrequency is small when the magnetic field is small, and thus the ion-ion collision rate will be comparable with the ion gyrofrequency, thereby invalidating the assumption of $E\times B$ dominated guiding center drifts.

In previous work, we have shown that the cross phase

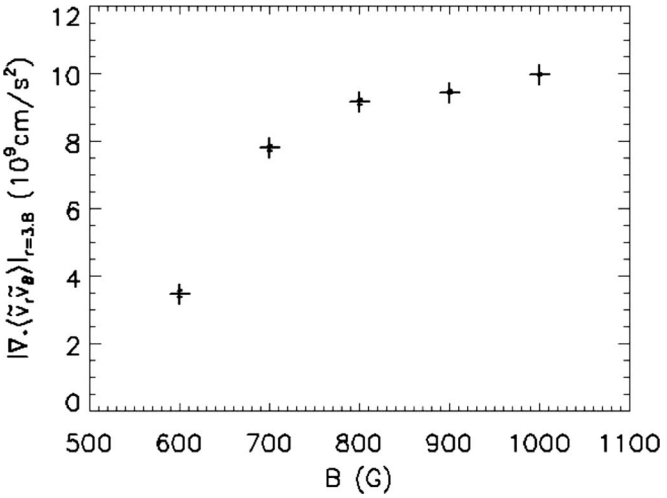

FIG. 5. Absolute value of the divergence of the turbulent Reynolds stress at the shear layer (~3.8 cm) for different magnetic fields.

between the radial and the azimuthal components of the velocity field is a key factor to determine the detailed turbulent Reynolds stress and hence the shear flow generation.[5] We have also investigated the evolution of the cross phase with the magnetic field to determine if it governs the variations in the turbulent Reynolds stress with magnetic fields. Figure 6(a) shows the radial profile of the turbulent Reynolds stress computed in the frequency domain from Eq. (1) shown as below,

$$\langle\tilde{v}_r\tilde{v}_\theta\rangle = \int_0^\infty 2\gamma_{\tilde{v}_r\tilde{v}_\theta}\cos\alpha_{\tilde{v}_r\tilde{v}_\theta}\sqrt{S_{\tilde{v}_r\tilde{v}_r}(f)}\sqrt{S_{\tilde{v}_\theta\tilde{v}_\theta}(f)}df, \qquad (1)$$

where $\gamma_{\tilde{v}_r\tilde{v}_\theta}$ is the cross coherence, $\cos\alpha_{\tilde{v}_r\tilde{v}_\theta}$ is the cross phase, and $S_{\tilde{v}_r\tilde{v}_r}(f)$ and $S_{\tilde{v}_\theta\tilde{v}_\theta}(f)$ are autospectrum of the radial and azimuthal velocity fields, respectively. As the magnetic field is increased, the negative divergence of the Reynolds stress needed to drive the shear slow increases in the region 3.5 cm$<r<$4 cm, which is precisely the location of the shear flow development. Using an approach similar to that described in detail in Ref. 4, an examination of the role of the velocity cross phase [Figs. 6(b) and 6(c)] shows that the Reynolds stress divergence is determined primarily by the evolution of the turbulent velocity cross phase. In particular, we note that when the cross phase is excluded from the turbulent Reynolds stress [Fig. 6(c)], there is much less variation near the shear layer. Our results therefore show that the turbulent velocity cross phase determines the variation in the turbulent Reynolds stress and that this cross phase is influenced by the strength of the magnetic field.

III. NEUTRAL GAS PRESSURE SCALING OF THE TURBULENCE DRIVEN SHEAR FLOW

Since the neutral gas pressure is also a possible parameter to control the transition to turbulence[9,10] and the ion-neutral drag can also damp out turbulence driven shear flow,[4] we have studied the evolution of the drift turbulence and sheared zonal flow for various neutral gas pressures, while keeping the other discharge conditions constant (a magnetic

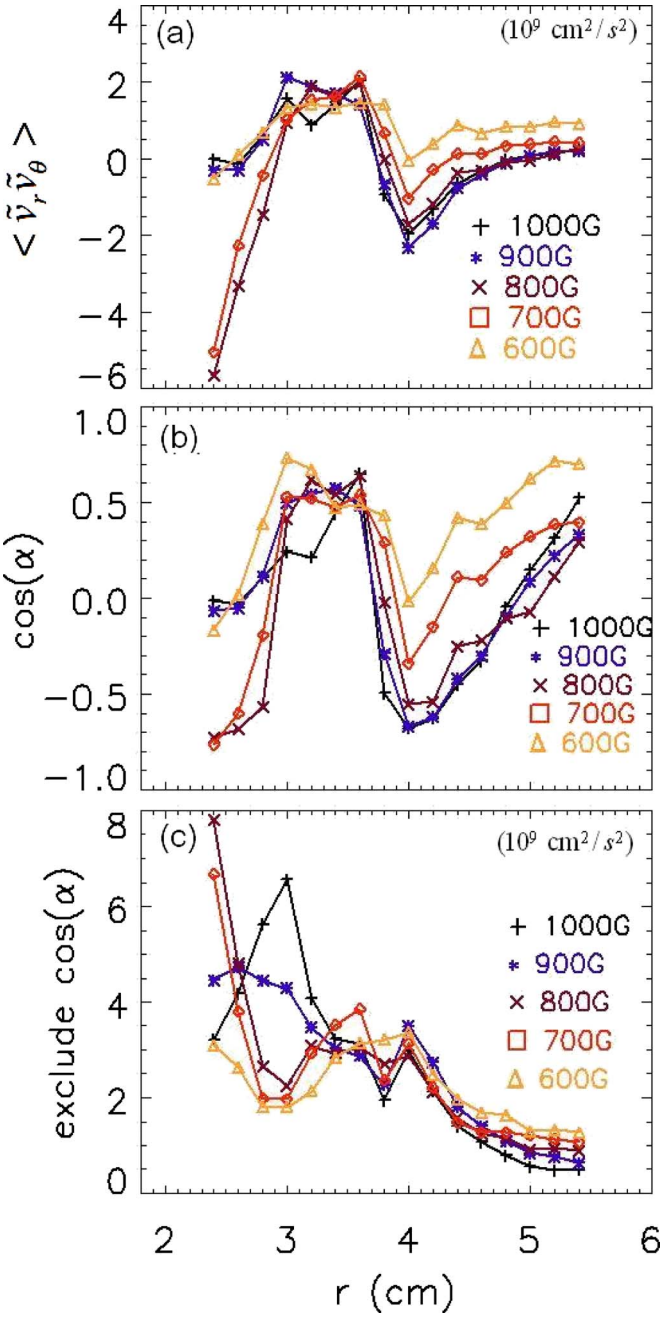

FIG. 6. (Color online) (a) Turbulent Reynolds stress computed in the frequency domain, (b) cosine of the cross phase, and (c) turbulent Reynolds stress with the cross phase excluded.

field of 1000 G and a source power of 1.5 kW were used for the work reported below). Figure 7 shows the radial distribution of the equilibrium plasma density for different neutral gas pressures, while Fig. 8 presents the variation in the density fluctuation amplitude and radial particle flux at 1000 G for the data obtained at $r=3$ cm. Each quantity is normalized by the corresponding value at 1000 G, 4 mTorr argon plasma condition. The results show that the plasma density increases with the neutral gas pressure, while the density fluctuation amplitude decreases with increasing neutral gas pressure. The radial particle flux peaks at 3.18 mTorr and decreases for higher pressures. Figure 9 shows the radial profile of the time-averaged azimuthal velocity fields at

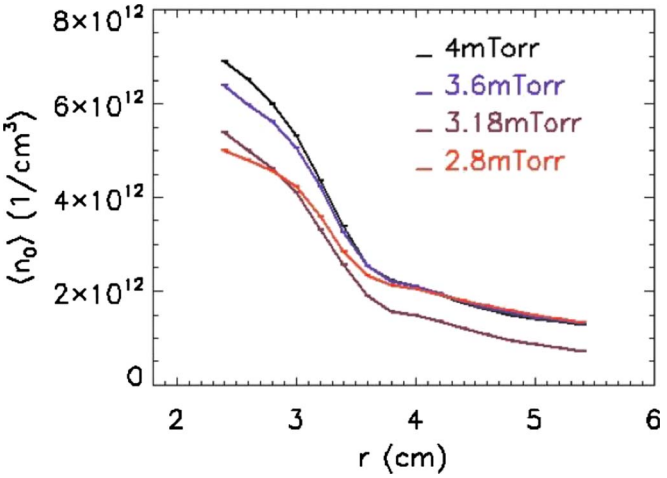

FIG. 7. (Color online) Equilibrium plasma density for different discharge pressures.

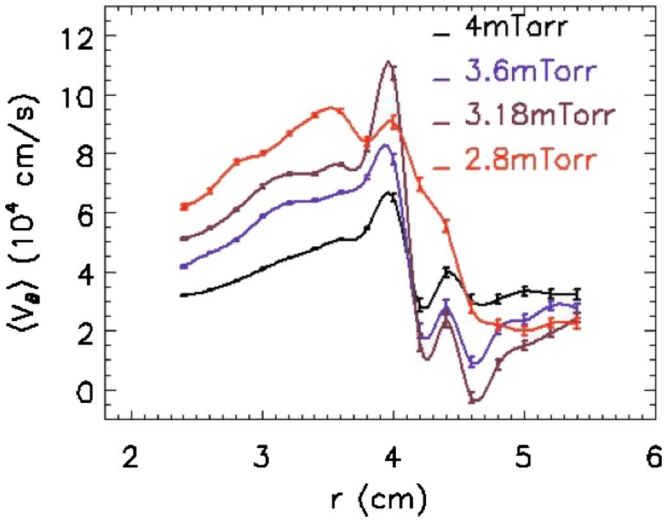

FIG. 9. (Color online) Time-averaged azimuthal velocity fields for different discharge pressures.

1000 G magnetic field for different neutral gas pressures. The results show that the shear flow velocity and the overall shearing rate decrease with the neutral gas pressure. The power spectra of both density fluctuations and floating potential at shear location ($\sim$3.8 cm) for various neutral gas pressures at 1000 G magnetic field are shown in Fig. 10. The amplitude of the 8–10 kHz drift fluctuations and the amplitude of the low frequency ($<$2 kHz) floating potential oscillation associated with the shear flow are both found to decrease as the neutral gas pressure is increased, consistent with our earlier observations, linking the shear flow to the 8–10 kHz components of the drift wave turbulence. Furthermore, we note that the width of the low frequency fluctuation component increases at low gas pressure, indicating that the temporal behavior of the shear flow becomes less coherent at lower gas pressure. These results are qualitatively consistent with an interpretation in which an increase in the neutral gas pressure reduces the turbulence amplitude (which is the nonlinear drive for the shear flow) and also increases the flow damping rate. As a result, at higher gas pressure, the shear flow becomes weaker. The divergence of the turbulent Reynolds stress $\nabla\cdot(\tilde{v}_r\tilde{v}_\theta)$ at the shear layer ($\sim$3.8 cm) decreases with an increase in the neutral gas pressure (Fig. 11), again consistent with expectations. An examination of the role of the cross phase and cross coherence shows that this decreased divergence is caused in large part by the variation in

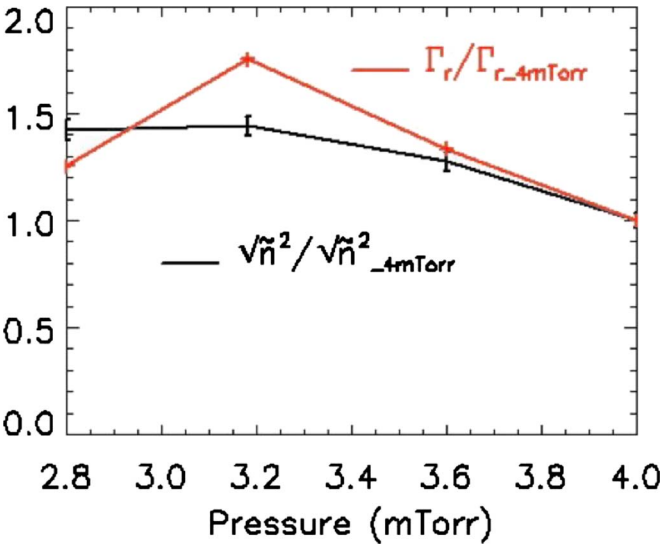

FIG. 8. (Color online) Density fluctuation amplitude (solid line) and radial particle flux (solid line and symbol +) at 1000 G magnetic field for different discharge pressures. Each data point is normalized by the corresponding value at 4 mTorr pressure.

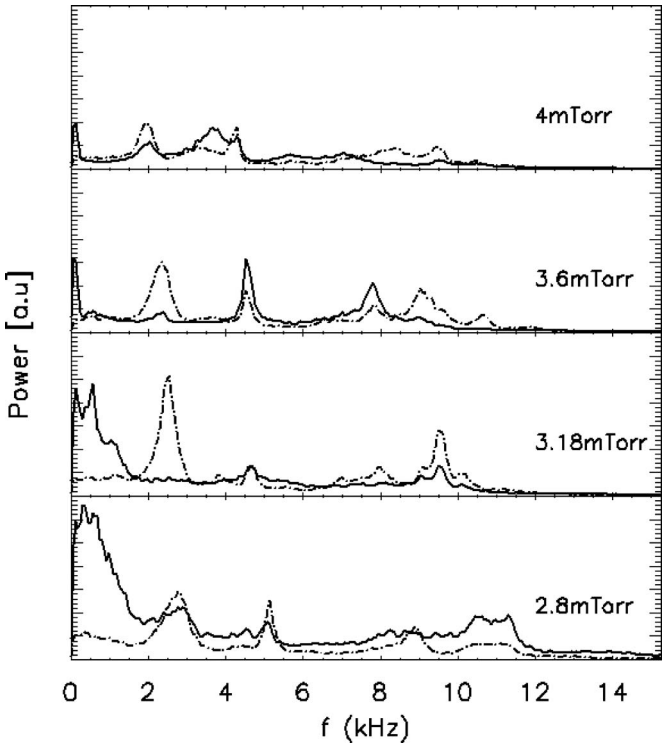

FIG. 10. Power spectra of density fluctuations (dashed line) and floating potential (solid line) at the shear layer ($\sim$3.8 cm), 1000 G magnetic field, for different discharge pressures.

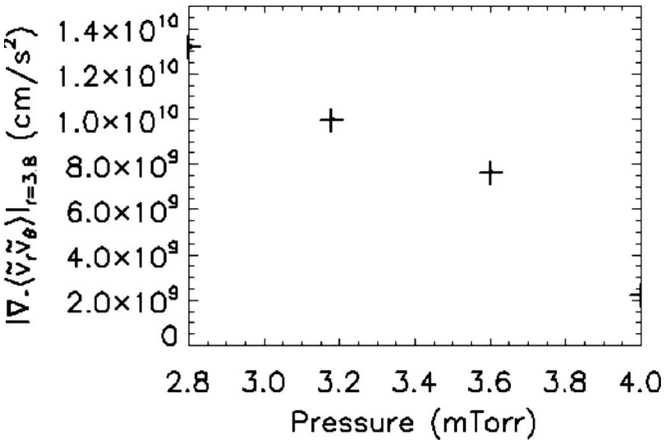

FIG. 11. Absolute value of the divergence of the turbulent Reynolds stress at the shear layer (~3.8 cm) for different discharge pressures.

the turbulent velocity cross phase with gas pressure (Fig. 12) together with the reductions in fluctuation amplitude discussed above.

IV. LINEAR STABILITY ANALYSIS WITH VARYING MAGNETIC FIELDS

Theory and numerical simulation of the coupled drift wave turbulence (DWT)/zonal flow (ZF) system show a critical gradient behavior in which the turbulence transport and the ZF are either stable or very weakly driven when the mean plasma pressure gradient is below a critical value. When this critical gradient is then exceeded, e.g., by increasing the heat flux through the system, the turbulent transport and the ZF are both predicted to then increase rapidly. This behavior then forces the system to stay close to the critical gradient, i.e., only small changes in the pressure gradient are needed to produce large changes in the turbulent flux. As a result, the central plasma conditions (which are essential for achieving energy gain in a fusion reactor) are determined in large part by the conditions at the plasma boundary, where other physics mechanisms associated with the transition to open magnetic field lines and plasma-wall interactions become important. This behavior has been observed in power balance studies performed in large confinement experiment and simulation,[16] but the key turbulence/ZF dynamics believed to be responsible for this behavior has never been measured experimentally in such a device. Here, we perform a linear stability analysis to provide the first such study for the coupled DWT/ZF system in a plasma experiment.

In order to determine the linear stability of fluctuations in the CSDX device, the collisional drift wave model of Hasegawa and Wakatani[17] is used. In cylindrical geometry, the model is written as

$$\frac{\partial \tilde{n}}{\partial t} + \frac{V^*(r)}{r}\frac{\partial \tilde{\phi}}{\partial \theta} + \omega_{\|}(\tilde{n} - \tilde{\phi}) = 0, \tag{2}$$

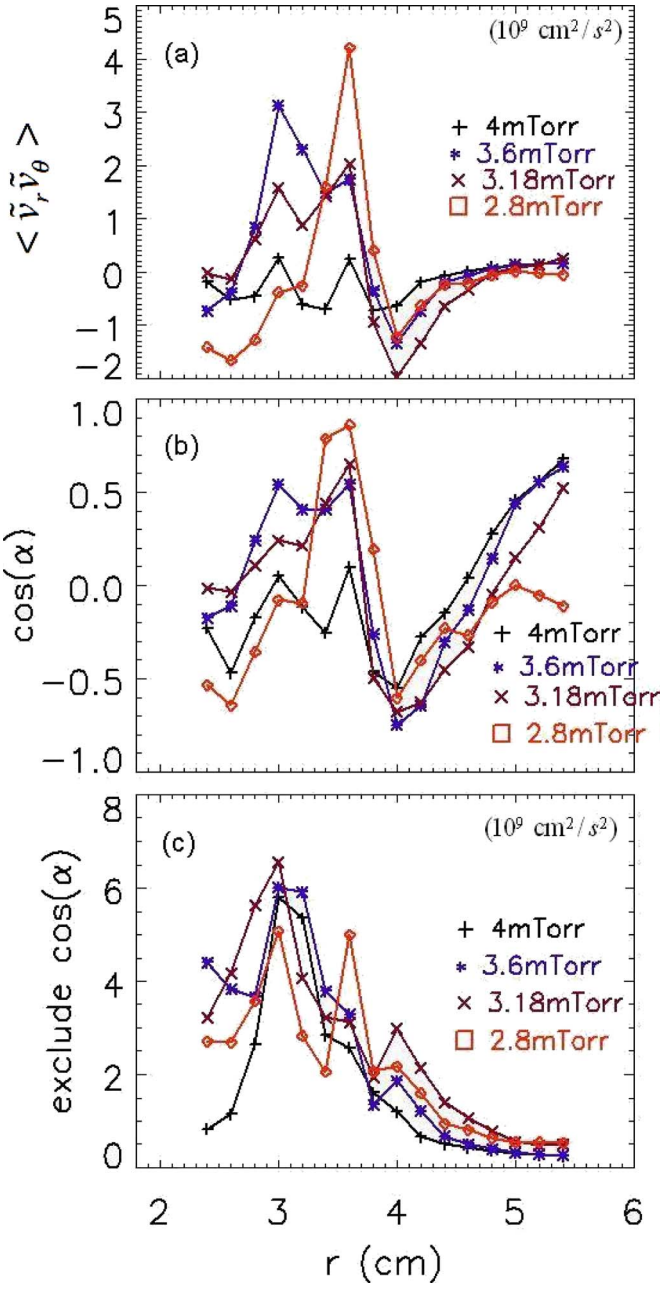

FIG. 12. (Color online) (a) Turbulent Reynolds stress computed in the frequency domain, (b) cosine of the cross phase, and (c) turbulent Reynolds stress with cross phase excluded.

$$\frac{\partial \nabla_\perp^2 \tilde{\phi}}{\partial t} + \frac{\omega_{\|}}{\rho_s^2}(\tilde{n} - \tilde{\phi}) + \upsilon_{i-n}\nabla_\perp^2 \tilde{\phi} - \mu_i \nabla_\perp^4 \tilde{\phi} = 0, \tag{3}$$

where $\tilde{n} = \delta n / n_0$, $\tilde{\phi} = e\delta\phi / T_e$, $V^*(r) = -\rho_s c_s d(\ln n_0)/dr$ is the electron diamagnetic velocity, $\omega_{\|} = k_{\|}^2 v_{Te}^2 / \nu_{ei}$ the so-called "adiabatic parameter," $\nu_{i\text{-}n}$ is the collision rate between ionized and neutral argon atoms,[18] $\mu_{ii} = 0.3\nu_{ii}\rho_i^2$ is the ion-ion collisional viscosity (which we take as a constant for simplicity in this analysis).[19] We make the further approximation that the equilibrium density can be described by a Gaussian $n_0(r) = n_0 \exp[-0.5(r/L_n)^2]$, then $V^*(r) = \rho_s c_s r / L_n^2$. Normalizing perpendicular spatial scales to ρ_s and time scales to L_n / c_s, the fluctuations can then be expanded in terms of a

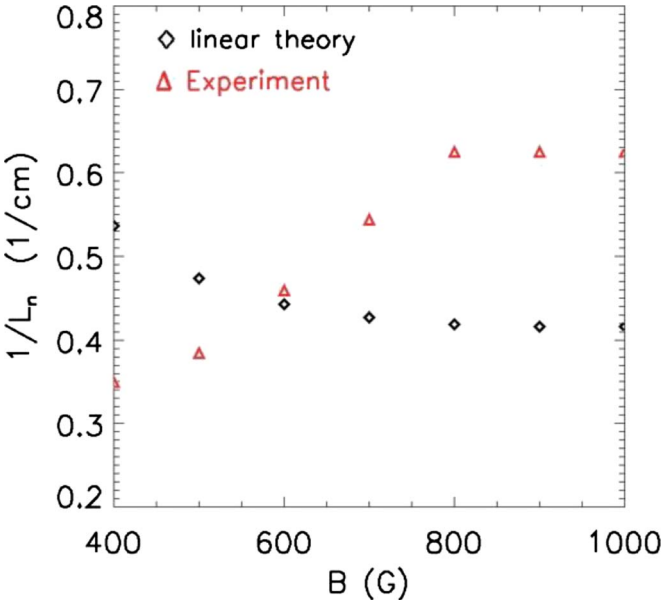

FIG. 13. (Color online) Inverse of the $m=1$ critical gradient scale length from both experiments and linear stability analysis for different magnetic fields.

Fourier series in θ and t, and Bessel functions in radius [e.g., $\tilde{\phi}(r,\theta,t)=\mathrm{Re}\Sigma_{mn}\tilde{\phi}_{mn}J_m(k_{mn}r)\exp\{i(m\theta-\omega_{mn}t)\}$], yielding a linear dispersion relation of the form

$$-ik_{mn}^2\omega_{mn}^2+\{\omega_{\|}(1+k_{mn}^2)+\nu_k\}\omega_{mn}-\omega_{\|}\left(m\frac{\rho_s}{L_n}-i\nu_k\right)=0, \tag{4}$$

where $\nu_k=(\nu_{i\text{-}n}+\mu_{ii}k_{mn}^2)k_{mn}^2$. The radial wavenumber k_{mn} is defined by requiring the fluctuations equal zero at $r=a$, such that $k_{mn}=X_{mn}/a$, where X_{mn} is the nth zero of $J_m(x)$. Solution of Eq. (3) using typical CSDX parameters ($a=10$ cm, $\nu_{i\text{-}n}=3$ kHz, $\mu_{ii}=4\times10^4$ cm^2/s, and $\omega_{\|}=100$ kHz) allows the determination of the complex eigenfrequencies ω_{mn}, the imaginary parts of which correspond to the linear growth rate of the eigenmode. Figure 13 shows the critical density gradient scale length calculated from linear stability analysis described above and measured in experiments for increasing magnetic fields from 400 G. As the magnetic field is increased, the critical value of $1/L_n(\propto\nabla n_0)$ for the $m=1$ mode to become unstable is reduced, while the experimental value of $1/L_n$ increases with the magnetic field. Therefore, when the magnetic field is higher than 600 G, the experimental density gradient scale length exceeds the critical gradient value and the linear instability grows. Combined with the results of previous sections showing that a development of ~10 kHz drift wave turbulence and strong shear exist at high magnetic fields (~700 G) but not at low magnetic field, these observations are consistent with a critical gradient behavior, namely, a rapid increase in the turbulence amplitude, particle flux, and turbulent-driven shear flow as the critical gradient is exceeded. As a result, one would expect the density profile to exhibit a very "stiff" behavior once the critical magnetic field is exceeded. This is indeed the case as seen by a careful examination of Fig. 1.

V. SUMMARY

In this paper, we have shown that as the relative strength of the convective derivative term to the viscous damping term is increased by increasing the magnetic field, a shear flow develops. The onset of this flow coincides with a rapid increase in the divergence of the turbulence Reynolds stress at the spatial location where the shear layer develops. In addition, the onset of the shear flow coincides with the rapid growth in the drift turbulence frequency components that are most strongly phase coherent with the slowly varying shear flow. As has been shown elsewhere,[20] this phase coherency is a necessary condition to transfer energy from the turbulence into the shear flow. Finally, the shear flow is damped when the net ion-neutral collision rate is increased. When coupled with previous studies showing that the turbulent Reynolds stress is self-consistent with the shear layer, these parametric variation studies provide additional strong evidence that the shear flow is indeed driven by turbulence and, in turn, regulates the turbulence and associated transport rates.

The results presented here also show evidence for a critical gradient behavior for the coupled weak drift turbulence-zonal flow system. When the density gradient scale length exceeds the critical gradient value from linear stability analysis, we observe a rapid increase in the drift wave turbulence. Since the turbulence, in turn, drives the shear flow, we would also expect a rapid onset of the shear flow. Then, when the shear flow becomes strong enough, it should then begin to affect the turbulence amplitude and correlation lengths via the shear decorrelation processes. The results shown in Figs. 2 and 3(b), i.e., experimentally observed variation in the turbulence amplitude, cross-field flux, and ZF shearing strength versus magnetic field for the 3.18 mTorr, 1.5 kW argon discharges have demonstrated such expected critical gradient behavior and provided a first study of critical gradient behavior for the coupled DWT/ZF system. We plan on a more detailed investigation of this important phenomenon which will be presented elsewhere.

The experimental results presented here have also shown that when the neutral gas pressure is increased, the increased ion-neutral drag begins to damp the shear flow. Recent simulations on edge momentum transport have shown that with an increase in the damping term (viscosity), the shear flow is reduced because the instability growth rate and the resulting nonlinear processes are all slowed down.[21] Our observations appear to be consistent with this simulation result.

The scaling properties of the ion momentum balance equation are also of interest and can quantitatively test if the shear flow is driven by turbulence for different plasma conditions. In order to estimate the ion viscosity and ion-neutral flow drag for various conditions, it is necessary to measure ion and neutral temperatures. We are planning this work and the results will be presented elsewhere.

ACKNOWLEDGMENTS

The authors wish to thank P. H. Diamond for many valuable suggestions and conversations. This research was performed under U.S. Department of Energy (DOE) Grant No. DE-FG02-06ER54871.

[1]P. H. Diamond, S.-I. Itoh, K. Itoh, and T. S. Hahm, Plasma Phys. Controlled Fusion **47**, R35 (2005).
[2]K. Itoh, S.-I. Itoh, P. H. Diamond, and T. S. Hahm, Phys. Plasmas **13**, 055502 (2006).
[3]C. Hidalgo, M. A. Pedrosa, L. García, and A. Ware, Phys. Rev. E **70**, 067402 (2004).
[4]C. Holland, J. H. Yu, A. James, D. Nishijima, M. Shimada, N. Taheri, and G. R. Tynan, Phys. Rev. Lett. **96**, 195002 (2006).
[5]Z. Yan, J. H. Yu, C. Holland, M. Xu, S. H. Muller, and G. R. Tynan, Phys. Plasmas **15**, 092309 (2008).
[6]M. Burin, G. R. Tynan, G. Y. Antar, N. A. Crocker, and C. Holland, Phys. Plasmas **12**, 052320 (2005).
[7]U. Kauschke and H. Schluter, Plasma Phys. Controlled Fusion **32**, 1149 (1990).
[8]U. Kauschke, Plasma Phys. Controlled Fusion **35**, 93 (1993).
[9]L. I and M. Wu, Phys. Lett. A **124**, 271 (1987).
[10]D. Weixing, H. Wei, W. Xiaodong, and C. X. Yu, Phys. Rev. Lett. **70**, 170 (1993).
[11]M. N. Rosenbluth and F. L. Hinton, Phys. Rev. Lett. **80**, 724 (1998).
[12]G. R. Tynan, A. D. Bailey III, G. A. Campbell, R. Charatan, A. de Chambrier, G. Gibson, D. J. Hemker, K. Jones, A. Kuthi, C. Lee, T. Shoji, and M. Wilcoxson, J. Vac. Sci. Technol. A **15**, 2885 (1997).
[13]M. Xu, G. R. Tynan, C. Holland, Z. Yan, S. H. Muller, and J. H. Yu, Phys. Plasmas **16**, 042312 (2009).
[14]G. Mckee, R. J. Fonck, D. K. Gupta, D. J. Schlossberg, and M. W. Shafer, Rev. Sci. Instrum. **75**, 3490 (2004).
[15]Z. Yan, Ph.D. thesis, University of California, 2009.
[16]D. R. Baker, C. M. Greenfield, K. H. Burrell, J. C. Deboo, E. J. Doyle, R. J. Groebner, T. C. Luce, C. C. Petty, B. W. Stallard, D. M. Thomas, M. R. Wade, and DIII-D Team, Phys. Plasmas **8**, 4128 (2001).
[17]A. Hasegawa and M. Wakatani, Phys. Rev. Lett. **50**, 682 (1983).
[18]N. A. Gondarenko and P. N. Guzdar, Geophys. Res. Lett. **26**, 3345, doi:10.1029/1999GL003647 (1999).
[19]S. I. Braginskii, Rev. Plasma Phys. **1**, 201 (1965).
[20]G. R. Tynan, R. A. Moyer, M. J. Burin, and C. Holland, Phys. Plasmas **8**, 2691 (2001).
[21]J. R. Myra, D. A. Russell, and D. A. D'Ippolito, Phys. Plasmas **15**, 032304 (2008).